Earth`s Cryosphere, 2015, vol. XIX, No. 4, pp. 17–28 **http://earthcryosphere.ru/**

PERMAFROST IN HAYES ISLAND, FRANZ JOSEF LAND ARCHIPELAGO

E.A. Slagoda[1,2], A.V. Krylov[3], K.A. Popov[1,2], O.L. Opokina[1,2], D.S. Drozdov[1,2,7], V.V. Rogov[1,4], A.N. Kurchatova[1,2], P.T. Orekhov[1], A.A. Ermak[1], T.V. Khodzher[5], I.V. Tomberg[5], M.Yu. Suslova[5], N.A. Zhuchenko[5], A.A. Abramov[6]

[1] Earth Cryosphere Institute, SB RAS, P/O box 1230, Tyumen, 625000, Russia; eslagoda@ikz.ru
[2] Tyumen State Oil and Gas University, 56 Volodarskogo str., Tyumen, 625000, Russia
[3] Joint Stock Company "Polargeo", V.O., 3/7, 24th Line, St. Petersburg, 199053, Russia
[4] Lomonosov Moscow State University, 1 Leninskie Gory, Moscow, 119991, Russia
[5] Limnological Institute, SB RAS, 3 Ulan-Batorskaya str., Irkutsk, 664033, Russia
[6] Institute of Physicochemical and Biological Problems in Soil Science, RAS, 2 Institutskaya, Pushchino, Moscow region, 142292, Russia
[7] Ordzhonikidze Russian State Geological Prospecting University, 23 Miklouho-Maklay str., Moscow, 117997, Russia

We report geocryological data from Hayes Island in the Franz Josef Land archipelago. The data include chemical and grain size compositions, species and age of shell faunas, cryostructures, and moisture content in samples from several boreholes and an outcrop, as well as micromorphology of thin sections and casts examined by optical and electron microscopy. Terraces of different ages are composed of talus, eluvium, and coastal Holocene sediments deposited in a cold climate. Changes of cryostructures and microstructures record epigenetic and syngenetic types of permafrost formed in marine, tidal and subaerial environments.

Structure, genesis, age, epigenetic permafrost, syngenetic permafrost

INTRODUCTION

Paleogeogaphic reconstructions and understanding of the Late Cenozoic geological and cryogenic history of Arctic islands and the Barentz-Kara shelf have been limited by data shortage until recently. No special geocryological research in the Franz-Josef Land archipelago has been undertaken through the 20th century, while the inferred permafrost parameters and types require empirical checks. The predictions [*Kondratiev, 1980*] are, namely: 15–40 cm thick active layer (thaw depth); –7 to –13 °C temperature of ice-free ground; massive or layered cryostructures; ice contents from 0.2 in sand to 0.4 in clay silt. The presumed permafrost origin is para-syngenetic in Quaternary deposits or epicryogenic in older pre-Quaternary rocks [*Ershov, 1988a*].

Field studies of 2010 in Hayes Island jointly by the Institute of Earth Cryosphere (IEC, Tyumen) and the Institute of Arctic Biology of the University of Alaska (Fairbanks, USA) showed a thaw depth of 0.34–0.68 m and a permafrost temperature of –8.0 to –10.5 °C, all estimates being slightly above but generally consistent with the predicted values [*Drozdov et al., 2011*].

The available data include buried and shore ice, snow fields, and wedge ice in permafrost at 50, 25–20, and 10–8.5 m high terraces in 2.5–5.0 m thick Holocene talus, marine, and glacial deposits [*Dibner, 1961, 1965*], as well as recently found 2–3 mm thick incipient ice wedges [*Drozdov et al., 2011*]. However, the cryostratigraphy of the area remains poorly investigated.

Periglacial deposition environments and types of permafrost are recorded in changes of cryogenic patterns in sedimentary sequences [*Katasonov, 1972, 1979*]. Syngenetic and epigenetic permafrost types differ in ice content, cryostructures, and relations between wedge ice and its hosts. Rocks that thaw and then naturally freeze back preserve their primary cryotic signatures as ice casts and postcryogenc structures [*Romanovsky, 1993; Kaplina, 2011a,b*].

The problem of discriminating between syngenetic and epigenetic permafrost arises when only small samples of frozen ground are available, such as cores with dispersed macroscopic characteristics. In this case, discrimination is guided by grain sizes and mineralogy of samples, as well as by their structures and textures controlled by permafrost [*Konishchev, 1981; Konishchev and Rogov, 1985; Ershov, 1988b; Rogov, 2009; Kurchatov and Rogov, 2014*]. Repeated thawing and freezing in syngenetic subaerial and coastal saline permafrost [*Badu, 2010*] deform the primary sedimentary bedding and clastic particles and produce new minerals, aggregates, and circular forms [*Zigert, 1981; Zigert and Slagoda, 1990; Slagoda, 1991; Slagoda et al., 2014a*]. Epigenetic permafrost is free from signatures of freezing-thawing cycles as freezing from above acts upon hard rocks [*Slagoda, 2005*], except for cryotic eluvium (rocks reworked in the active layer) [*Konishchev, 1981*].

Traces of permafrost formation in the micromorphology of epigenetically and diagenetically frozen saline sediments, which are viscoplastic at negative

temperatures, remain very little investigated [*Ershov, 1988b; Zayonchek and Usov, 2003*]. Meanwhile these structures have implications for cryotraceology (systematizing permafrost signatures) as a basis for reconstructing the history of deposition and freezing in high-latitudes and on the Arctic shelf.

STUDY AREA AND METHODS

Study area

Hayes Island belongs to the Franz-Josef Land archipelago lying between 80° and 82 °N in the northeastern Barents shelf (Fig. 1). The archipelago consists of 400–490 m high volcanic-sedimentary plateaus cut by faults with up to 1000 m of vertical offset, the uplifted and subsided blocks being, respectively, islands and water between them [*Ershov, 1988a*]. Hayes Island is composed of Jurassic and Cretaceous mudstones, sandstones, and siltstones with basaltic lavas and sills from 5 to 40 m thick [*Dibner, 1965*] and Mesozoic dolerite dikes [*Karyakin et al., 2009*]. The dipping or flat basaltic bodies armor sandstones and mudstones creating cuesta-like topography. Dikes form low (within 100 m) hogbacks striking in the northwestern direction and border terraced depressions, with elevations 0–50 m, descending into the sea. The slopes are drained by a network of small creeks fed from melting snow fields and glaciers which flow into shallow valleys incised in low coastal terraces.

The elevated parts of the dike hogbacks are occupied by an ice dome (Gidrografov) rising up to 242 m, and their slopes are cut by low-angle steps, where sandstone bedrock is incised by modern creeks tracing ice retreat. The ice dome was larger in the past, judging by the presence of blocks and boulders transported to short distances on depressed surfaces. There are modern perennial snow fields, locally buried under aeolian sand, on northern slopes, rocky or ice benches, and in creek valleys. The ice-free part of the island belongs to the climate zone of Arctic desert.

Methods

Samples were taken from three 3 to 10 m deep boreholes (BH) and an outcrop cut in a creek valley between a 40–80 m high dike and a glacier (Fig. 2). Core samples were studied in terms of cryostructures, moisture contents, grain sizes, as well as dissolved salts and chemistry of melt ice, and its oxygen and heavy hydrogen isotope compositions (H. Meyer, Alfred Wegener Institute of Polar and Marine Research in Potsdam, Germany). Fauna studies were: stratigraphy; species of mollusks and their habitats (A.V. Krylov, CJSC Polargeo); ages of shells found in core samples (T. Goslar, Poznan Radiocarbon Laboratory).

Mineralogy and cryostructures (micromorphology) were examined in thin sections and replicas of oriented samples, under optical and scanning electron microscopes, at the Institute of Earth Cryosphere (Tymen, Russia). The results were used to infer the environments of deposition and freezing of sediments, as well as to trace signatures of permafrost in the Arctic coastal plains [*Slagoda and Kurchatova, 2008; Slagoda et al., 2013, 2014a,b*]. In syngenetic permafrost, they are layered and reticulate cryostructures, cracks, and circular forms produced by spatial differentiation of particles. The latter may be simple radiated forms or complex concentric aggregates inside larger structures. Post-cryogenic processes produce voids and pores as ice lenses melt in natural conditions and cause disintegration and lumping of sediments. Epigenetic permafrost commonly shows layered or re-

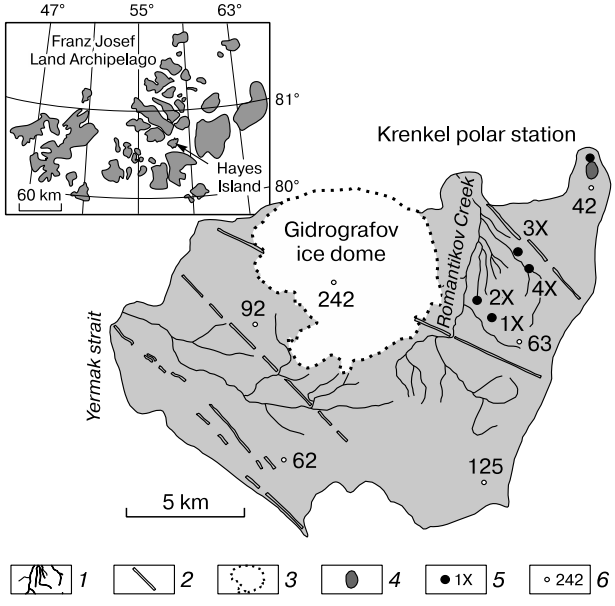

Fig. 1. Location map of study area.

1 – river drainage; *2* – dikes; *3* – glacier; *4* – lake; *5* – boreholes and outcrop cut; *6* – elevation above sealevel.

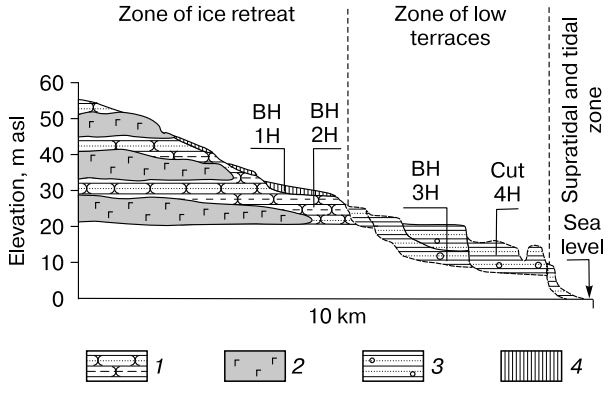

Fig. 2. Location of boreholes.

1 – Jurassic sandstones and siltstones; *2* – basaltic sills; *3* – marine and coastal deposits; *4* – talus, eluvium, and slope wash.

ticulate cryostructures and cryoturbation inherited from or superposed upon the primary sedimentary bedding, as well as diagenetic or primary postcryogenic structures. After epigenetic permafrost thaws, voids in rocks often coalesce and leave displaced or compacted layers, traces of dehydration or iron impregnation along cracks.

RESULTS

Zone of ice retreat (*Gidrografov glacier*). Sampling was from 1 m (1H) and 3 m (2H) deep boreholes drilled on 30–27 m high steps dipping at 5–10° to the west, in a valley side in central Hayes Island (Figs. 1, 2). On the step surfaces, which are mostly free from ice and partly covered with lichen and moss, there are scattered debris, heaved and fractured plates, sandstone boulders, and siderite nodules (up to 2 m). Small gullies between large (more than 20 m) polygons, which are split, in turn, by seasonal desiccation cracks into 0.1–0.3 m patches and blocks, produce patterned ground.

BH 2H (80°35′35″ N, 57°54′13″ E), interval 1.9–3.0 m: frozen bedrock (Table 1; Figs. 3, *A, B*; 4, *c–e*).

Layer 1: hard cross-bedded fine sandstones and siltstones, with 8–13 % clay content and low ice content, cut by ice-filled thin dipping cracks;

Layer 2: weathered ice-rich sandstones and sands with lenticular cryostructures;

Layers 3, 4 in BH 2H and layers 1–3 in BH 1H: subaerial sediments (silt, clay silt, and silty sand) on bedrock, with blind cross bedding parallel to ground surface and with lenses of weathered ferruginated sandstones and fine plant detritus; high ice content; massive, lenticular, reticulate, basal, and ataxitic cryostructures (Table 1). From 29.0 to 41.5 % of coarse silt particles in sand and silty sand and up to 40 % of particles smaller than 0.005 mm in clayey silt; low salinity; marine-type salt ion composition with $Cl > SO_4 > HCO_3$ and $Na + K > Mg > Ca$ (Table 2).

Zone of low terraces. Sampling was from 10 m borehole 3H drilled in terraces dipping westward (seaward) at 3–5° and from outcrop cut 4H.

BH 3H (80°36′23″ N, 57°54′35″ E) is located on a 20-m high terrace incised by the Romantikov Creek and its tributaries, as well as by gullies along frost cracks. Patterned ground is produced by large polygons extending parallel to 2.5–3.0 m high escarpments dipping toward the creek valley. There are flat-bottom ravines and triple junctions of frost cracks with narrow bars between them. The sediments contain abundant mollusk shells.

The BH 3H section consists of silty sands and sandy or clayey siltstones (Table 1), with 17–25 % and 30.0–56.2 % of coarse silt particles, respectively (Fig. 3). Bluish-gray, tobacco-gray or less often yellowish-brownish frozen sediments contain integer or broken bivalve shells and numerous bluish-black mottles or curved bands of polychaeta tissues degraded *in situ* (Fig. 4). The sediments are highly saline and become encrusted with salt as ice moisture evaporates. Salt ion composition is of marine type with $Cl > SO_4 > HCO_3$ and $Na + K > Mg > Ca$ (Table 2).

The section includes five layers with erosive boundaries, which differ in lithology and cryostratigraphy.

Layer 1 (3.5 m): numerous angular to rounded clasts and pebbles of weathered basalts, dolerites, sandstones, mudstones, and quartz; shells of bivalves *Mya truncata* Linnaeus, 1758 and *Astarte crebricostata* (MacAndrew & Forbes, 1847); low ice contents; massive or fine reticulate cryostructures and cryoturbation; 0.2–15.0 mm thick ice lenses (Fig. 4, *j–o*).

Layer 2 (2.9 m): cross-bedded sand at base lying over an eroded surface of the underlying sediments; silts and lenses or layers of yellowish silt and sand with weathered dolerite in the middle; thick-walled shells, a piece of a thin-walled pearl shell of *Margarites* cf. *groenlandicus* gastropod (Gmelin, 1791), and a shrub branch with bark (possibly, willow) in silts (Fig. 3; 4, *h–j*); high ice content; ataxitic and lenticular cryostructures with inclined or horizontal lenses (Table 1).

Layer 3 (2.7 m): predominant sands with thick-walled shells of *Mya truncata* Linnaeus, 1758 and bluish-black burrows of polychaetes delineating the eroded layer surface (Fig. 4, *g*); ice content decreasing upsection; lenticular cryostructures at base, massive or crust-like (around shells) and lenticular ones in the middle, and lenticular cryostructures with voids in ice lenses near top.

Layer 4 (0.43 m): variegated sands with ochre and black stains; contorted bedding; ground veins; high ice contents; crust-like and reticulate cryostructures.

Layer 5 (0.52 m): yellowish sand and silt with basal and ataxitic cryostructures (Fig. 4, *f*); unfrozen dry sand to depths of 0.4 m.

Outcrop cut 4H, 100 m away from BH 3H, exposes the stratigraphy of a low terrace (14–15 m above the sealevel), which extends in a narrow strip along the Romantikov Creek and is separated from the 20-m terrace by snow fields. Gullies cut the terrace into 30–50 m wide blocks rising 4–5 m above the creek valley. There are deflated sands, fractured blocks, and scattered shells on the surface; organic remains include whale vertebras and a rounded and cracked tree trunk in the creek channel.

The 4H section (Table 1) includes an active layer (seasonally thawing) and three permafrost layers: ice-rich plane-bedded silt and clay silt (1); ice-poor sand and silt with cross bedding dipping toward creek valley (2, 3), with damaged shells of *Mya truncata* Linnaeus, 1758, *Astarte placenta* (Morch, 1869) and an oblique ice lens with chaotic ice bubbles and inclusions of the host soil on the margins (Fig. 3).

Table 1. **Cryostratigraphy of drill sections**

Borehole, layer	Depth, (thickness), m	Lithology	Cryostructure	Moisture content, %
1	2	3	4	5
BH 1H, layer 1	1.0–0.64 (0.36)	Dark and light gray silty sand with low-angle lenticular bedding; scattered landwaste; vertical elongate clasts of gray sandstones and siltstones and brown lenses of plant detritus	Lenticular, irregular reticulate, wavy; 0.2 to 2.5 cm thick ice lenses; inclusions of silt, detritus, and air bubbles in 4–6 cm thick inclined ice layers	65.0
BH 1H, layer 2	0.64–0.48 (0.16)	Gray yellowish sand with interbeds of brown silt and inclusions of ochre sandstone clasts	Inclined lenticular, irregular reticulate, basal near top; ice lenses thickening up the section	78.1
BH 1H, layer 3	0.48–0.0 (0.48)	Yellow-brown silt with minor ochre stains and plant detritus	Coarse lenticular (lenses to 2.5 cm) and reticulate. Ice pockets (5 cm) with up to 1 cm voids above. Frozen to depth 0.35 m; unfrozen tixotropic part of active layer on top	94.3
BH 2H, layer 1	2.9–1.9 (1.0)	Hard fine sandstones interbedded with dark gray siltstones; ochre stains and tongues; grading smoothly to sediments above	Massive with scarce thin (1–3 mm) lenses across or parallel to bedding; iron stains and whitish crusts of carbonate salts on walls of cryogenic voids	11.4–19.0
BH 2H layer 2	1.9–1.25 (0.65)	Gray sand and soft sandstones and siltstones with distinct sedimentary bedding	Fine lenticular in clay silt and silt; up to 2 cm thick ice lenses in sand	36.9
BH 2H, layer 3	1.25–0.6 (0.65)	Dark gray silt and clay silt; minor ochre stains; small plant detritus; lenses of gray clay silt and brown clay; discontinuous horizontal and low-angle cross bedding	Fine lenticular, with scarce horizontal or oblique lenses; iron stains at ice contacts; to 0.5 cm thick oblique ice lenses in cross-bedded sands	14–19
BH 2H, layer 4	0.6–0.0 (0.6)	Yellowish-brown silt and sand; light-gray silt with wavy bedding; yellow stains and plant detritus; brown clay silt lenses, layers; cryoturbation	Pure fine lenticular and massive; frozen to depth 0.4 m and unfrozen and dry above; modern active layer	29.4
BH 3H, layer 1	6.5–10.0 (3.5)	Saline gray sand and silt; black stains and circles along polychaeta burrows; flattened rounded pebbles and angular clay pieces below; landwaste (gray carbonate and ochre sandstones and siltstones); large thick-walled shells above; fuzzy top	Massive; scarce dipping ice lenses, broken or parallel; thin vertical and horizontal lenses making a reticule (Figs. 2, 3)	25–31
BH 3H, layer 2	3.62–6.5 (2.9)	Saline tobacco and dark gray fine sand and sandy silt; black stains; below: dipping 0.5–2.0 cm thick layers of sand and dark gray silt with shells; in the middle: thin layers and pockets (0.10–0.15 m) of yellowish-brown silt with basaltic landwaste; clasts of thin-walled shells; integer or partly degraded shells and sporadic plant remnants (a willow branch with bark); salt encrustation on permafrost; fuzzy top	Inclined and horizontal lenticular; ataxitic (granular ice with sand inclusions and voids) in interbeds of yellowish-brown silt	37–41; 95–100
BH 3H, layer 3	0.95–3.62 (2.7)	Sand with silt interbeds; below: cross-laminated bluish-gray silty sand; above: saline blind-laminated tobacco-gray silt and sand with thick-walled integer or broken shells; black dipping or vertical thin layers and circles of polychaeta burrows, and sections along and across them; salt encrustation on permafrost; fuzzy top	Below: dipping ice lenses, to 0.3 cm, with voids; in the middle: thin lenses parallel to cross lamination; above: thin ice lenses and open cracks, with hoar on walls	25–49
BH 3H, layer 4	0.52–0.95 (0.43)	Bluish-black fine sand with black stains and shell clasts; black stains around tongues of tobacco-gray sand with ochre stains penetrating from above; distinct wavy base cut by small and narrow cracks	Massive with ice pockets and crusts, and thin ice lenses; transitional layer	56
BH 3H, layer 5	0.0–0.52 (0.48)	Brownish and yellowish-gray sand and silt with ochre iron stains; inclusions, tongues, and pockets	Below: basal and ataxitic; above: thin lenticular and irregular reticulate to massive; post-cryogenic layeed unfrozen rocks, to 0.34 m; modern active layer	77–98
Cut 4H, layer 1	3.2–2.2 (1.0)	Brownish-gray silt with blind bedding produced by lenses or thin (2 cm) layers of yellowish sand with iron and black stains; fuzzy top	Below: coarse wavy bedding with 2–5 cm thick ice lenses; above: basal, ataxitic, irregular reticulate, with 0.5 cm ice lenses	–

Continued table 1

1	2	3	4	5
Cut 4H, layer 2	2.2–1.25 (1.0)	Dark gray silt and ochre sand; integer or broken thin- and thick-walled shells; low-angle parallel bedding produced by 8–20 cm thick layers of silt and 2–5 cm ochre sand	Massive and crust-like (around shells)	–
Cut 4H, layer 3	1.25–0.5 (0.75)	Ochre sand and brownish clayey sand; dolerite landwaste; integer or broken shells; distinct cross bedding (2–10 cm layers); base dipping toward creek	Massive; 60 cm long and 3–10 cm oblique irregular ice lens at depth 0.80–1.25 m	–
Cut 4H, layer 4	0–0.5 (0.5)	Pale yellow massive sand; shell clasts; top dipping toward creek	Unfrozen; modern active layer	–

Ice samples analyzed for oxygen and hydrogen stable isotopes, salinity, and chemistry show low salinity (20.7 mg/l TDS), chloride-sulfate-sodic ion compositions (Table 3), and relatively high contents of some trace elements: Be, B, Cr, Mn, Se, and Cd (Table 4). Ice stores cultivable psychrophile bacteria (725 CFU/ml) that form mostly orange, yellow, and pink pigmented colonies.

Variations in cryostructures and ice contents in BH 1H and 2H record the presence of an active layer (seasonally thawing) and permafrost: transitional layer (relict active layer) [*Shur, 1988*], subaerial layer, and weathered and hard bedrock. The 20-m terrace section includes an active layer and permafrost (layer 5), a transitional layer (4), and layers 3, 2, 1 of saline permafrost. The 4H section includes an active layer and permafrost, both different from those in the 20-m terrace (Fig. 2).

DISCUSSION

The obtained data have implications for deposition environments, cryostratigraphy, permafrost types and ages.

Origin and types of permafrost in zone of ice retreat

The sections of dipping steps (BH 1H, 2H) comprise several layers evident from changes in cryostructures and ice contents: a 0.48 m thick modern active layer (seasonally thawing), a 0.16 m transitional (fossil active) layer and three layers of frozen sediments, including subaerial silt and sand with bedding parallel to the dipping surfaces that contain bedrock clasts and plant detritus (layer 3), and weathered and hard bedrock (layers 1 and 2).

Permafrost types were inferred from microstructure (micromorphology) analysis.

Hard siltstones and sandstones (layer 1) have distinct cross and horizontal bedding produced by distribution of clay and iron hydroxides and by orientations of clastic particles and elongate lignitic remnants. The sediments consist of angular to rounded detrital feldspar, quartz, and weathered bedrock. The bedding is crosscut and displaced by frost cracks (merged linear voids filled with fine particles) producing irregular reticulate cryostructure. Magnification of different strengths reveals cracks in clasts, even in the samples that did not experience mechanic effects.

Weathered siltstones and sandstones (layer 2) preserve parallel bedding but contain abundant fractured angular and detrital feldspar clasts. Fine-grained sediments (Fig. 5, *a–c*) have complex microstructures with 0.3–0.5 mm isometric aggregates encircled by flat detrital grains and enclose isometric or elongate cryogenic voids (to 2.5 mm) with rough walls.

Variations in cryostructures, fracture patterns in clasts and aggregate-circular microstructures record effects of cyclic freezing and thawing that decay down the section. Therefore, weathered and hard Mesozoic rocks are interpreted as cryogenic eluvium. Bedrock alluvium became saline when it was flooded by seawater prior to the formation of glaciers in the archipelago [*Dibner, 1998*].

Subaerial sand (layer 3, BH 1H and 2H) mainly consists of angular clasts and detritus and often forms complex concentric aggregates. It encloses inclined plant remnants, fresh or substituted by clay, and round cryogenic voids with rough walls. The microstructures, along with sedimentary bedding parallel to the dipping surface, fresh plant remnants, and high ice contents, indicate subaerial origin and syngenetic freezing of sediments.

Thus, high terraces and steps in Hayes Island are surfaces exposed to subaerial denudation and deposition. Sediments have low contents of seawater salts but mostly receive salts from bedrock.

Origin and types of permafrost in zone of low terraces

The section of the 20-m terrace consists of five cryogenic layers: an active layer (5), seasonally thawing with unfrozen and frozen parts; a transitional layer (4); and three permafrost layers (3, 2, 1). The division according to macroscopic features is consistent with that indicated by microstructures.

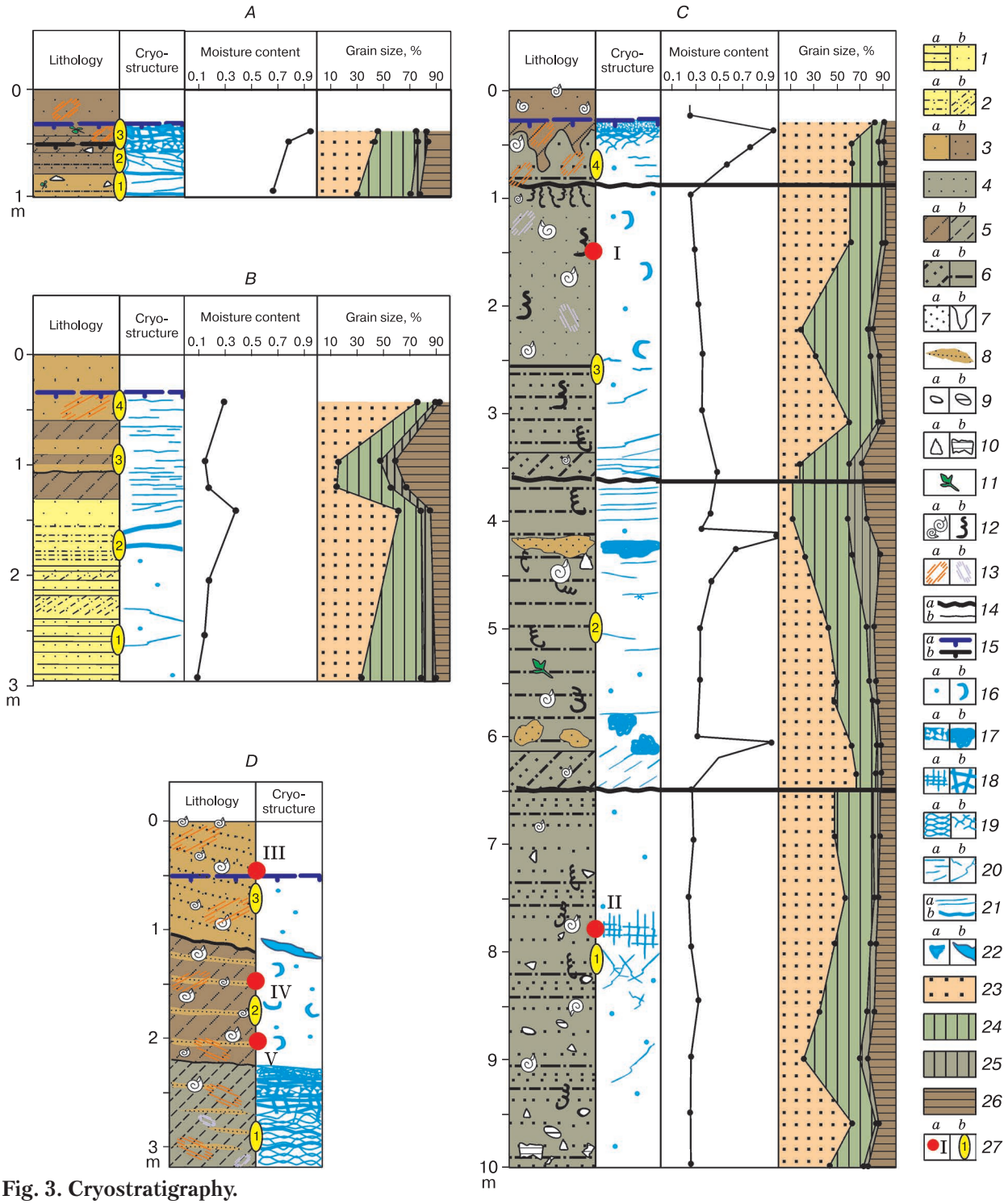

Fig. 3. Cryostratigraphy.

A: BH 1H, 30 m asl; *B*: BH 2H, 28 m asl; *C*: BH 3H, 20 m asl; *D*: outcrop cut 4H, 17 m asl.
1 – hard (*a*) and weathered (*b*) cemented sandstone; *2* – plane- (*a*) and cross-bedded (*b*) siltstones; *3* – non-saline gray (*a*) and brownish clayey-silty (*b*) sand; *4* – saline clayey-silty sand; *5* – non-saline (*a*) and saline (*b*) silt; *6* – cross bedding of saline sand and silt (*a*), plane-bedded silt and clay silt (*b*); *7* – cross-bedded sand (*a*) and soil injections or veins (*b*); *8* – lenses and layer of non-saline sand; *9* – pebble of hard rocks (*a*), rounded pebble of siltstones and mudstones (*b*); *10* – angular clasts of sandstones (*a*) and mudstones (*b*); *11* – plant remnants, branches; *12* – mollusk shells (*a*), traces of degraded polychaeta (*b*); *13* – ochre (*a*) and bluish (*b*) stains and tongues; *14* – erosive (*a*) and deposition (*b*) boundaries; *15* – base of modern (*a*) and fossil (*b*) active layers; *16–22* – cryostructures: massive (*a*) and crust-like (*b*) (*16*), ataxitic (*a*) and basal (*b*) (*17*), fine reticulate (*a*) and coarse lenticular (*b*) (*18*), regular (*a*) and irregular (*b*) reticulate (*19*), lenticular (*a*) and cryoturbated (*b*) (*20*), fine layered (*a*) and coarse lenticular (*b*) (*21*), enclosed structures (*a*) and ice lenses (*b*) (*22*); *23–26* – grain sizes (mm): 1.0–0.05 (*23*), 0.05–0.01 (*24*), 0.01–0.005 (*25*), <0.005 (*26*); *27* – shell samples for dating (*a*) and layer number (*b*). Points I–V are ^{14}C dates (calendar ages): (7140 ± 50) kyr BP, BH 3H, depth 1.5 m, marine bivalves (I); (9770 ± 50) kyr BP, BH 3H, depth 7.8 m, marine bivalves (II); (7510 ± 50) kyr BP, cut 4H, depth 0.45 m, marine bivalves (III); (8040 ± 50) kyr BP, cut 4H, depth 1.6 m, clasts of marine bivalves (IV); (8170 ± 50) kyr BP, cut 4H, depth 2.0 m, clasts of marine bivalves (V).

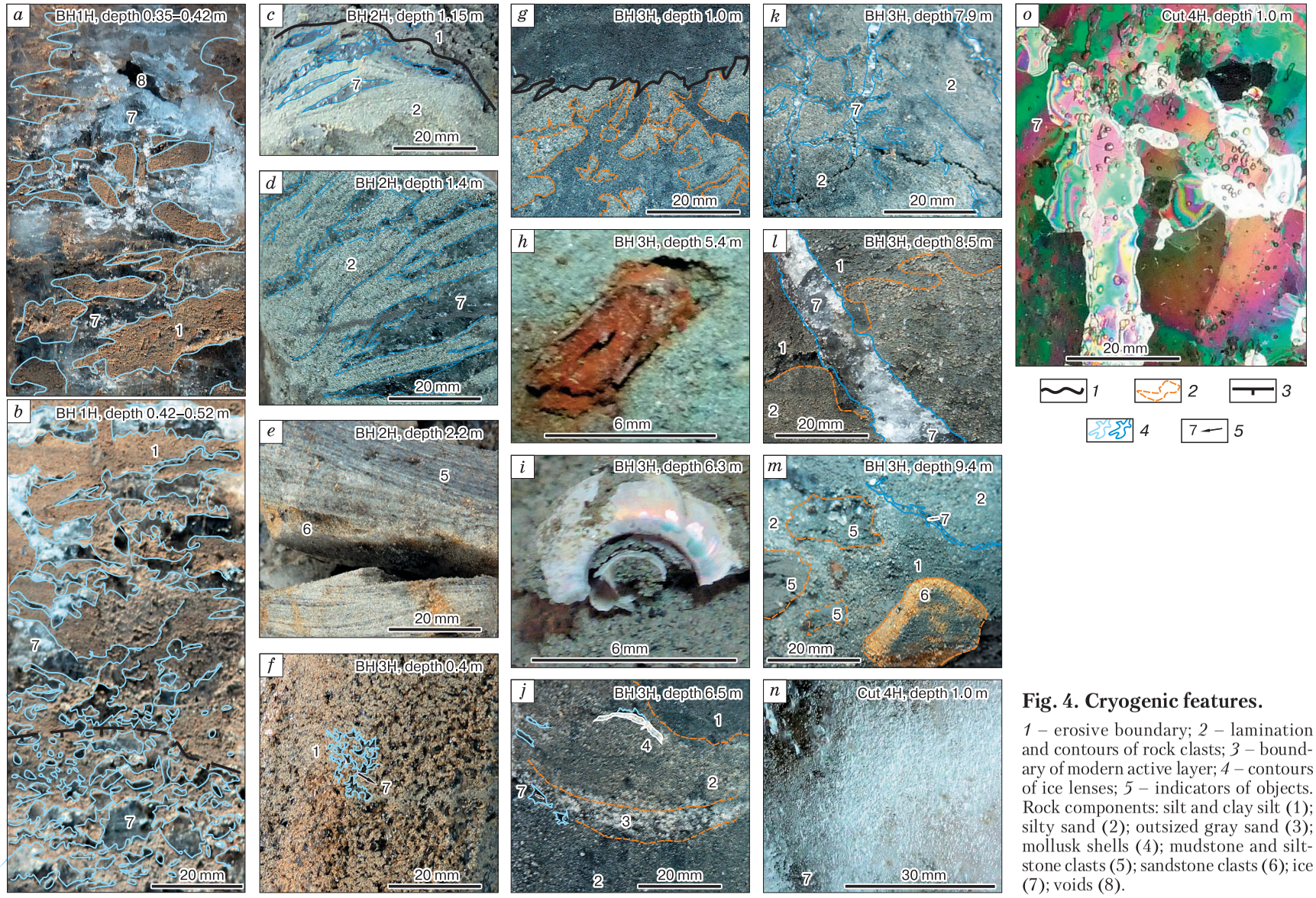

Fig. 4. Cryogenic features.

1 – erosive boundary; *2* – lamination and contours of rock clasts; *3* – boundary of modern active layer; *4* – contours of ice lenses; *5* – indicators of objects. Rock components: silt and clay silt (1); silty sand (2); outsized gray sand (3); mollusk shells (4); mudstone and siltstone clasts (5); sandstone clasts (6); ice (7); voids (8).

Table 2. **Ion composition**

Borehole	Depth, m	Ion contents, % eq.							Ion sum, mg/100 g	C_{tot},%
		HCO_3	Cl	SO_4	Ca	Mg	K	Na		
2H	0.6	12.1	60.4	27.5	2.3	8.1	2.1	87.5	4.04	0.279
	1.0	–	–	–	–	–	–	–	–	1.262
	1.2	5.9	65.0	29.1	0.7	4.4	1.7	93.2	12.38	1.363
	1.4	–	–	–	–	–	–	–	–	0.482
	2.5–2.55	6.9	51.8	41.3	1.3	6.7	2.4	89.6	6.66	–
3H	0.32	–	–	–	–	–	–	–	–	0.350
	0.71	–	–	–	–	–	–	–	–	0.610
	1.0	–	–	–	–	–	–	–	–	0.558
	1.4–1.5	4.2	74.9	20.9	3.9	7.3	3.9	84.9	29.66	0.585
	2.2–2.27	0.7	86.4	12.9	2.9	6.7	2.7	87.7	48.62	0.950
	2.5	–	–	–	–	–	–	–	–	0.885
	2.52	–	–	–	–	–	–	–	–	0.480
	3.0–3.2	0.7	88.3	11.0	2.5	4.9	2.1	90.5	63.18	0.665
	3.5	–	–	–	–	–	–	–	–	1.162
	4.3	–	–	–	–	–	–	–	–	0.562
	5.0	0.7	87.4	11.9	2.2	6.7	2.5	88.6	57.62	–
	5.5	–	–	–	–	–	–	–	–	0.882
	6.35–6.4	0.8	88.3	10.9	2.5	6.1	2.6	88.8	32.41	–
	6.95	–	–	–	–	–	–	–	–	0.767
	7.5	–	–	–	–	–	–	–	–	0.663
	7.92	–	–	–	–	–	–	–	–	0.768
	8.5–8.6	0.6	87.6	11.8	3.2	5.1	2.2	89.5	60.26	0.873
	9.0	–	–	–	–	–	–	–	–	1.153
	9.6	–	–	–	–	–	–	–	–	0.597
	10.0	–	–	–	–	–	–	–	–	0.897

Note. Dash means not determined.

Table 3. **Oxygen and deuterium isotope composition of ice from outcrop cut 4H-2010**

Sample number	Position	Section	$\delta^{18}O$, ‰ (vs. SMOW)	δD, ‰ (vs. SMOW)	d_{exc}
31806	7/5	4H-2010-1A	–14.82	–110.8	7.7
31807	8/5	4H-2010-1B	–14.84	–110.5	8.2

Note. d_{exc} is deuterium excess.

Table 4. **Major- and trace-element compositions of molten ice lens**

pH	γ, S/m	Ion contents, % eq.							Ion sum, mg/l	Suspended matter, g/l	PO_4	NO_3	Org. COD
		HCO_3	Cl	SO_4	Na	K	Ca	Mg			mg/l		
6.08	$4.65 \cdot 10^{-3}$	24	49	27	50	5	25	20	20.69	1.29	0.04	8.08	0.72

Trace elements (ppm), from ICP–MS data*

Li	Be	B	Al	Ti	V	Cr	Mn	Fe	Co	Ni	Cu	Zn	As	Se	Sr	Mo	Cd	Ba
–	13.37	64.42	2.50	0.36	0.51	77.52	98.92	0.16	1.53	0.44	3.73	0.03	–	10.26	1.66	–	5.72	–

Note. Ice was molten immediately before analysis.
γ is specific critical electrical conductivity at liquid temperature 25 °C.
COD is chemical oxygen demand that indirectly measures the amount of organic compounds in water (mass of oxygen consumed per liter of solution).
* Mass Spectrometry with Inductively Coupled Plasma on an *Agilent 7500ce* analyzer.
Dash means contents below detection limit.

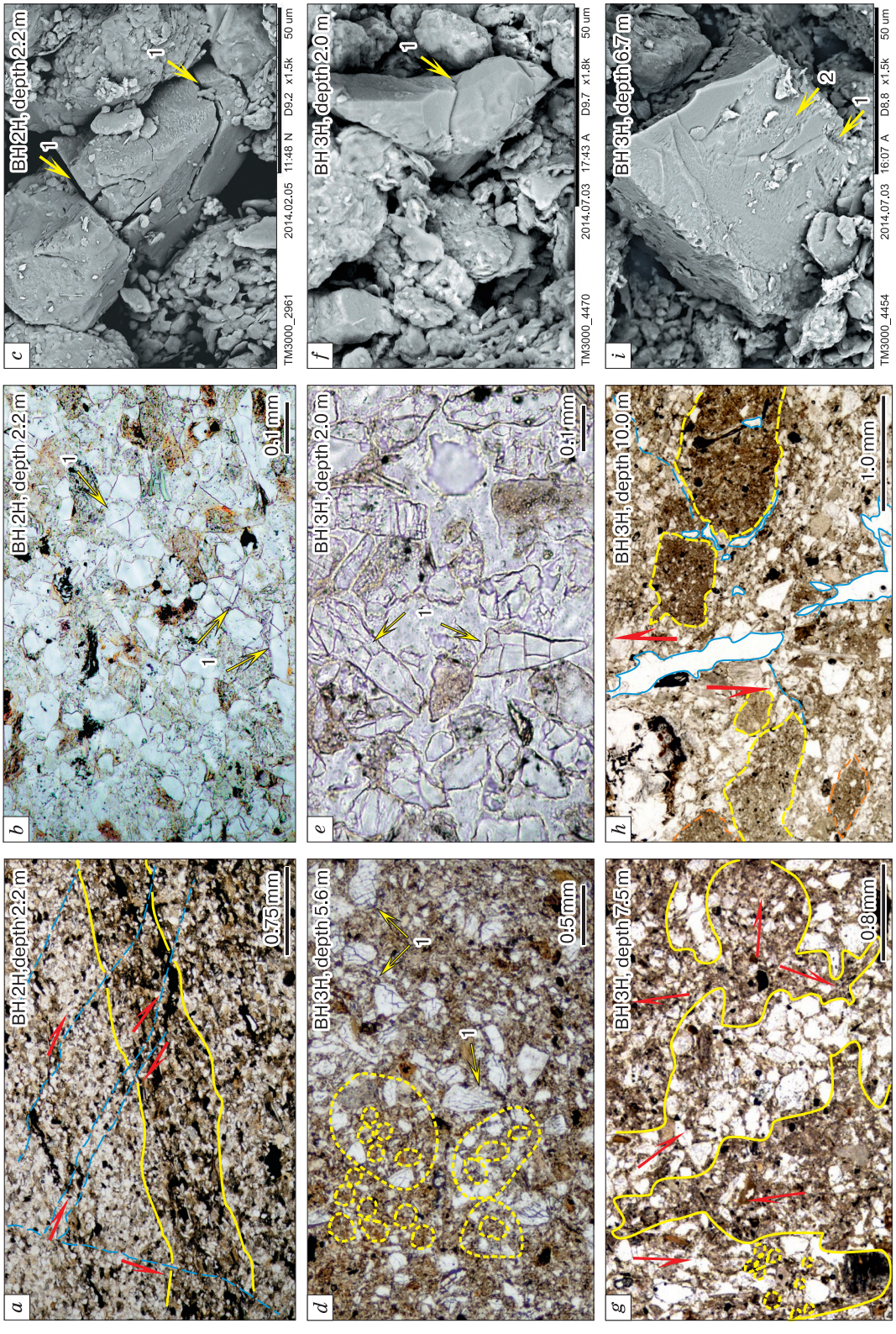

Fig. 5. Micromorphology.

a–c – cryogenic eluvium, BH 2H, layer 1; *d–f* – syngenetic permafrost, BH 3H, layer 3; *g–i* – epigenetic permafrost, BH 3H, layer 1. *1* – layer boundaries; *2* – contours of clasts and rounded pebbles; *3* – particles forming aggregates and circles; *4* – contours of cryogenic voids (*a*), post-cryogenic coalescent cracks (*b*); *5* – displacement direction; *6* – indicators of objects. Numerals at arrows are cracks and fractured clasts (1) and traces of chemical weathering (2).

Layer 1: chaotic patchy distribution of clasts typical of ice rafting; absence of fractured clasts and prevalence of simple clay aggregates (smaller than 0.05 mm); plastic contorted bedding; traces of strong chemical weathering in angular to rounded clasts of rocks and minerals common to marine environments; cryogenic voids with smooth walls which crosscut, offset, and bend the layers; rounded mudstone pebbles with different orientations corresponding to lenticular or reticulate cryostructures (Fig. 5, *g–i*). These microstructures lack evidence of cyclic freezing and thawing and cryogenic weathering. Therefore, diagenetically altered saline sediments of layer 1 were frozen epigenetically.

Layer 2: fractured detrital feldspar and quartz clasts, with primary sedimentary bedding obscured by numerous circular forms and complex aggregates (0.25–0.80 to 2 mm); integer carbonate shells of foraminifera coexisting with degraded tissues of polychaeta, plant detritus, either fresh or replaced by colloids and iron sulfides; redeposited clasts of siderite concretions and shells. These microstructures correspond to syndepositional cyclic freezing and thawing. Therefore, the saline sediments of layer 2 form syngenetic permafrost recorded also in cryostuctures.

Layer 3: fractured detrital mineral grains; complex aggregates of matrix material in fine-grained layers; foraminifera and fresh poorly degraded tissues of polychaeta; newly formed iron sulfides and carbonates; numerous irregular and tortuous voids with rough walls between aggregates producing lenticular-reticulate cryostructures (Figs. 5, *d–f*). These features correspond to syndepositional cyclic freezing and thawing of sediments. Ice content decreasing up the section and voids in ice lenses may result from cooling and subaerial evaporation of ice moisture from rocks near the surface.

Depositional and permafrost environments of low terraces

High salinity of *frozen deposits in the 20-m terrace*, as well as presence of polychaeta remnants, abundant mollusk shells, and dispersed clasts indicate their marine origin. *Astarte crebricostata* (MacAndrew & Forbes, 1847) and *Mya truncata* Linnaeus, 1758, whose shells are found in layers 1 and 3, are extant mollusks in moderately cold and cold Arctic seas at shelf depths from 3 to 200 m [*Merclin et al., 1979; Krylov et al., 2009*]. Layer 2 contains shells of *Margarites* cf. *groenlamdicus* (Gmelin, 1791) that live now at shelf depths 0–100 m in moderately cold Arctic seas [*Troitsky, 1979*], and remnants of terrestrial plants (a shrub branch with bark). The habitats of mollusks and the presence of chaotically dispersed clasts suggest deposition of layers 1 and 3 in conditions of ice rafting in sea gulfs deeper than those where layer 2 was deposited in a shallow-water shelf environment.

The history of marine deposition reconstructed from macroscopic and microscopic cryogenic features and permafrost types was as follows:

– layer 1 was deposited and then altered in a sea gulf; it was partly eroded when emerged during regression and frozen epigenetically;

– layer 2 was deposited at alternating subaerial/submarine shore and shelf conditions and froze and thawed repeatedly; freezing was syngenetic, in the presence of frozen substrate (layer 1);

– layer 3 was deposited in a relatively deep sea gulf but froze syngenetically while frozen layer 2 remained preserved on the shelf bottom; correspondingly, the deposition was faster than that of layer 2 and occurred in a colder climate.

Therefore, the 20-m terrace formed when sea depths changed and the former shelf emerged.

Silt layer 1 exposed in cut 4H on the *15-m terrace incised in the 20-m terrace* has distinct horizontal bedding, high ice contents, and layered or reticulate cryostructures, unlike layers 1 and 2 in BH 3H located at the same depth (Fig. 3). Layers 2 and 3 in cut 4H dip toward the creek valley and have distinct cross bedding, ochre color of sand, lower salinity and low ice contents. There are abundant clasts and integer shells of *Astarte crebricostata* (MacAndrew & Forbes, 1847) and *Mya truncata* Linnaeus, 1758 that live at shelf depths from 3 to 200 m and in shallow gulfs of the Arctic shelf. Judging by abundant fragments of redeposited shells and cryostructures, the 15-m terrace formed in a shallow gulf by erosion of the 20-m terrace, while its deposits became syngenetically frozen in shallow-water or subaerial conditions.

The layered sands of the 15-m terrace enclose an ice lens at the base, with its composition and structure indicating aeolian and nival processes involved in the terrace formation. The dip of the lens, its irregular shape, chaotically dispersed air bubbles, inclusions of the host sand, as well as coarse crystalline structure (Fig. 4, *n, o*) are typical of free water frozen in a confined space, or cave-thermokarst ice according to *Vtyurin* [*1975*]. Ice of this kind lies under modern aeolian sand in Hayes Island and under frozen talus on degrading ice-rich Arctic coasts [*Streletskaya et al., 2012*]. The oxygen and hydrogen isotope composition of the Hayes Island ice lens differs from that of wedge ice in northern West Siberia [*Vasil'chuk, 2006*] and falls into the field of infiltration meteoric water [*Kritsuk, 2010*], though this information is insufficient to infer the ice origin [*Konishchev et al., 2014*]. The relative contents of major ions ($Cl > > SO_4 > HCO_3$) and the presence of B and Mn in ice are as in seawater [*Fotiev, 1999*]. High concentrations of Cr, Be, and Cd in the ice lens, compared with those in Spitsbergen ice [*Korzun, 1985*] and in ground ice from the northern Yenisei catchment [*Opokina et al., 2014*], indicate an input of surface waters rich in com-

ponents leached from weathered dolerite and basalt. The presence of pigmented microbial colonies is common to Artic snow fields.

Therefore, the ice lens results from freezing of confined snow-melt and surface waters that drain dolerites and the 20-m saline coastal terrace. The small width of the 15-m coastal terrace, as well as the dip of subaerial sediments, evidence that the creek valley was flooded during ingression while the sea retreated progressively.

Age of coastal terraces

Layers 1–3 separated by eroded surfaces in the 3H section were deposited within the 9.8 to 7.1 kyr interval, as inferred from mollusk shells buried *in situ* (Fig. 3). Thus, the 20-m terrace formed during Boreal and Atlantic stages of the Holocene in conditions of changing sealevel when the shelf emerged. The deposits of the 15-m terrace contain 8.1 to 7.5 kyr shells (Atlantic stage), but the presence of redeposited thick-walled shells and whale bones suggest a younger age of the terrace corresponding rather to the second half of the Holocene [*Dibner, 1998*].

CONCLUSIONS

Geocryological studies of permafrost in drill sections of Hayes Island in the Franz Josef Land archipelago provide evidence on cryostratigraphy and origin of sediments. High dipping terraces in the zone of ice retreat are composed of Mesozoic bedrock affected by frost weathering (cryogenic eluvium) and thin syngenetically frozen talus. Low terraces are composed of saline marine sediments laying under subaerial deposits. The permafrost section of the 20-m terrace consists of three layers (from bottom to top):

– epigenetically frozen deposits of a sea gulf with products of ice rafting;

– beach and shelf sediments syngenetically frozen in submarine and subaerial conditions of a shoaling gulf;

– deposits of a relatively deep sea gulf syngenetically frozen upon permafrost in submarine conditions.

Permafrost of the 15-m terrace formed in a setting of ingression consists of syngenetically frozen sediments of a shallow gulf that flooded creek valleys and subaerial talus and aeolian sand.

The 20-m coastal terrace formed while the sea depths in the gulf changed and the sea retreated between 9.8 and 7.1 kyr BP, during the Boreal and Atlantic stages of the Holocene.

The study was supported by grant 14-17-000131 from the Russian Science Foundation.

References

Badu, Yu.B., 2010. Geocryology. Moscow University Press, Moscow, 528 pp. (in Russian)

Dibner, V.D., 1961. Anthropogene Paleogeography of the Franz Josph Land in the light of radiocarbon dating results: New data. Dokl. AN SSSR 138 (4), 893–894.

Dibner, V.D., 1965. Late Pleistocene and Holocene History of the Franz Josef Land. NIIGA Transactions XXIV, Moscow, pp. 300–319.

Dibner, V.D. (Ed.), 1998. Geology of Franz Josef Land. Meddelelse, Oslo, No. 146, 191 pp.

Drozdov, D.S., Slagoda, E.A., Abramov, A.A., et al., 2011. Permafrost Research in Hayes Island (Franz Josef Land Archipelago): Preliminary Results. Univ. Kniga, Moscow, pp. 52–59.

Ershov, E.D. (Ed.), 1988a. Geocryology of the USSR. Nedra, Moscow, 358 pp. (in Russian)

Ershov, E.D. (Ed.), 1988b. Permafrost Microstructures. Moscow University, Moscow, 182 pp. (in Russian)

Fotiev, S.M., 1999. Formation of the ion-salt composition of natural waters in Yamal. Kriosfera Zemli III (2), 40–65.

Kaplina, T.N., 2011a. Ancient Alas Complexes of Northern Yakutia (Part 1). Kriosfera Zemli XV (2), 3–13.

Kaplina, T.N., 2011b. Ancient Alas Complexes of northern Yakutia (Part 2). Kriosfera Zemli XV(3), 20–30.

Karyakin, Iu.V., Lyapunov, S.M., Simonov, V.A., et al., 2009. Mesozoic igneous complexes in the Franz Josef Land archipelago, in: Geology of High-Latitude Areas. Proc. XLII Tectonic Workshop, GEOS, Moscow, Book 1, pp. 257–263. (in Russian)

Katasonov, E.M., 1972. Types of permafrost and problems of geocryology, in: Geocryological and Hydrogeological Studies in Siberia. Institute of Permafrost, Yakutsk, pp. 5–16. (in Russian)

Katasonov, E.M. (Ed.), 1979. Structure and Isotope Ages of Alas Deposits in Central Yakutia. Nauka, Novosibirsk, 96 pp. (in Russian).

Kondratieva, K.A., 1980. Permafrost conditions of the Franz Josef Land Archipelago. Merzlotnye Issled. XIX, 76–101.

Konishchev, V.N., 1981. Formation of Frozen Disperse Ground. Nauka, Novosibirsk, 196 pp. (in Russian)

Konishchev, V.N., Rogov, V.V., 1985. Methods of Permafrost Studies. Moscow University Press, Moscow, 185 pp. (in Russian)

Konishchev, V.N., Golubev, V.N., Rogov, V.V., Sokratov, S.A., Tokarev, I.V., 2014. Experimental study of the isotopic fractionation of water in the process of ice segregation. Earth Cryosphere (Kriosfera Zemli) XVIII (3), 3–10.

Korzun, A.V., 1985. Ice sheet evolution in Arctic islands: Paleoclimate conditions, in: Popov, A.I. (Ed.), Late Cenozoic History of Permafrost in Eurasia, Nauka, Moscow, pp. 150–155. (in Russian)

Kritsuk, L.N., 2010. Ground Ice in West Siberia. Nauchnyi Mir, Moscow, 352 pp. (in Russian)

Krylov, A.V., Zarkhidze, D.V., Marke, R., 2009. Cenozoic mollusks of the Russian Arctic and their stratigraphic significance, in: Basic Problems of the Quaternary: Results and Prospects. Proc. All-Russia Workshop on Quaternary, Novosibirsk, pp. 302–304. (in Russian)

Kurchatova, A.N., Rogov, V.V., 2014. Grain sizes and morphology of cryotic soils: New methods and approaches. Inzhenernye Izyskaniya, No. 5–6, 58–63.

Merklin, R.L., Zarkhidze, V.S., Ilyina, L.B., 1979. Pliocene-Pleistocene Marine Mollusks in Northeastern European USSR: Identification Manual. Nauka, Moscow, (Transactions, Paleontological Institute, 173), 96 pp. (in Russian)

Opokina, O.L., Slagoda, E.A., Tomberg, I.V., et al., 2014. Sea-level change and its record in the composition and structure of wedge ice in the Yenisei lower reaches. Led i Sneg, No. 2, 82–90.

Rogov, V.V., 2009. Fundamentals of Cryogenesis. Geo Publishers, Novosibirsk, 208 pp. (in Russian)

Romanovsky, N.N., 1993. Fundamentals of Cryogenesis in the Lithosphere. Moscow State University, Moscow, 336 pp. (in Russian)

Shur, Yu.L., 1988. Shallow Permafrost and Thermokarst. Nauka, Novosibirsk, 213 pp. (in Russian)

Slagoda, E.A., 1991. Microstructure of ice-complex deposits in Northern Yakutia (a case study of Bykov Peninsula), in: Soil Cryology, IFKHBPP, Pushchino, pp. 38–47. (in Russian)

Slagoda, E.A., 2005. Micromorphological Signatures of Cryogenesis in Late Cenozoic Sediments: Implications for the History of Permafrost (in Russian). Author's Abstract, Doctor Thesis (Geology & Mineralogy), IKZ SO RAN, Tyumen, 48 pp.

Slagoda, E.A., Kurchatova, A.N., 2008. Micromorphological analyses of main genetic permafrost types in West Siberia, in: Proc. 9th Intern. Conf. on Permafrost (NICOP). Fairbanks, Alaska, USA, pp. 1659–1663.

Slagoda, E.A., Leibman, M.O., Khomutov, A.V., Orekhov, P.T., 2013. Cryolithologic construction of the first terrace at Bely island, Kara sea (Part 1). Kriosfera Zemli XVII (4), 11–21.

Slagoda, E.A., Kurchatova, A.N., Popov, K.A., et al., 2014a. Cryolithologic structure of the first terrace: microstructure and evidence of cryolithogenesis, Bely Island, Kara Sea (Part 2). Kriosfera Zemli XVIII (1), 12–22.

Slagoda, E.A., Kurchatova, A.N., Opokina, O.L., Tomberg, I.V., Khodzher, T.V., Firsova, A.D., Rodionova, E.V., Popov, K.A., Nikulina, E.L., 2014b. Cryostratigraphy of terrace I in Bely Island, Kara Sea: Permafrost and climate history (Part 3). Earth Cryosphere (Kriosfera Zemli) XVIII (3), 33–45.

Streletskaya, I.D., Vasiliev, A.A., Slagoda, E.A., et al., 2012. Ice wedges in Sibiryakov Island (the Kara Sea). Bull. Moscow University, Ser. 5, Geography 3, 57–63.

Troitsky, S.L., 1979. Pleistocene Marine Deposits of Siberian Plains. Siberian RAS, Novosibirsk, (IGiG Transactions, Issue 430), 293 pp. (in Russian)

Vasil'chuk, Yu.K., 2006. Ice Wedges: Uneven Cyclicity, Structure, and Ages. Moscow State University, Moscow, 404 pp. (in Russian)

Vtyurin, B.I., 1975. Ground Ice in the USSR. Nauka, Moscow, 215 pp. (in Russian)

Zayonchek, V.G., Usov, V.A., 2003. Diagenetic freezing of coastal deposits. Bull. St.-Petersburg University, Ser. 7. Geol. Geogr. 3 (23), 83–86.

Zigert, KH.G., 1981. Mineral formation in periglacial conditions, in: Structure and Thermal Regime of Permafrost. Nauka, Novosibirsk, pp. 14–21. (in Russian)

Zigert, KH.G., Slagoda, E.A., 1990. Results of permafrost studies of ice complexes in Yakutia, in: Quaternary Stratigraphy and Events in Eurasia and Pacific Regions. YaSC, Yakutsk, pp. 82–84. (in Russian)

Received February 9, 2015